Author Manuscript

Author Manuscript

Author Manuscript

Author Manuscript

HHS Public Access

Author manuscript

Cell Rep. Author manuscript; available in PMC 2017 September 27.

Published in final edited form as:

Cell Rep. 2017 September 05; 20(10): 2468–2479. doi:10.1016/j.celrep.2017.08.048.

The Ulk3 kinase is critical for convergent control of cancer associated fibroblast activation by CSL and Gli

Sandro Goruppi[1,2], **Maria-Giuseppina Procopio**[3], **Seunghee Jo**[1,2], **Andrea Clocchiatti**[1,2], **Victor Neel**[4], and **G. Paolo Dotto**[1,3,#]

[1]Cutaneous Biology Research Center, Massachusetts General Hospital, 149 Bldg. 13th St. Charlestown 02129 MA, USA [2]Department of Dermatology, Harvard Medical School, Boston 02125 MA, USA [3]Department of Biochemistry, University of Lausanne, 155 Chemin des Boveresses, Epalinges, CH-1066, Switzerland [4]Department of Dermatology, Massachusetts General Hospital, Boston 02114 MA, USA

SUMMARY

The connection between signaling pathways activating cancer associated fibroblasts (CAFs) remains to be determined. Metabolic alterations linked to autophagy have also been implicated in CAF activation. CSL/RBPJ, a transcriptional repressor that mediates Notch signaling, suppresses gene expression program(s) leading to stromal senescence and CAF activation. Deregulated Gli signaling can also contribute to CAF conversion. Here we report that compromised CSL function depends on Gli activation for conversion of human dermal fibroblasts into CAFs, separately from cellular senescence. Decreased CSL up-regulates the expression of the Ulk3 kinase, which binds and activates Gli2. Increased Ulk3 also induces autophagy, which is unlinked from Gli and CAF activation. Ulk3 up-regulation occurs in CAFs of several tumor types and Ulk3 silencing suppresses the tumor enhancing properties of these cells. Thus, Ulk3 links two key signaling pathways involved in CAF conversion and is an attractive target for stroma-focused anti-cancer intervention

Keywords

Tumor microenvironment; Cancer stroma; CAF (Cancer associated fibroblast); CSL/RBPJ; Autophagy; Gli

[#]Correspondence to GPD, (lead contact) paolo.dotto@unil.ch.

SUPPLEMENTAL INFORMATION

Supplemental information includes five figures, extended experimental procedures and four tables.

AUTHOR CONTRIBUTIONS

S.G., M.P., S.J. and A.C. performed the experiments and contributed to analysis of the results. V.N. provided clinical samples. S.G. and G.P.D. designed the study and wrote the manuscript.

Publisher's Disclaimer: This is a PDF file of an unedited manuscript that has been accepted for publication. As a service to our customers we are providing this early version of the manuscript. The manuscript will undergo copyediting, typesetting, and review of the resulting proof before it is published in its final citable form. Please note that during the production process errors may be discovered which could affect the content, and all legal disclaimers that apply to the journal pertain.

Author Manuscript Author Manuscript Author Manuscript Author Manuscript

INTRODUCTION

Stepwise acquisition of genetic alterations is implicated in epithelial tumor development, yet many of these changes can be found in apparently normal tissues, pointing to the importance of concomitant stromal changes (Bissell and Hines, 2011; Hanahan and Weinberg, 2011; Martincorena et al., 2015). Notch signaling controls cell fate commitment, differentiation and tumorigenesis (Allenspach et al., 2002; Artavanis-Tsakonas et al., 1999; Dotto, 2009). While, Notch tumor suppressive function in stratified epithelia is well established (Dotto, 2008), recent evidence indicates an opposite role in stromal fibroblasts (Hu et al., 2012; Junttila and de Sauvage, 2013; Procopio et al., 2015). Specifically, the CSL/RBP-Jκ protein (CSL), a transcriptional repressor mediating Notch signaling, is key for the negative control of cancer associated fibroblast (CAF) activation. Deletion of CSL gene in the mesenchymal skin compartment of mice results in multifocal keratinocyte tumor development preceded by dermal atrophy, matrix alterations and inflammation (Hu et al., 2012). CSL loss in primary human fibroblasts results in a similar CAF phenotype, that is associated with a p53-dependent program of cellular senescence (Procopio et al., 2015). The concomitant down modulation of CSL and p53 activities leads to the expansion of altered stromal fibroblasts and cancer cells as seen in *field cancerization*, a condition of major clinical significance consistent of multiple and recurrent tumors (Dotto, 2014).

The Hedgehog (Hh) pathway is linked to the development of several types of epithelial cancers (Rubin and de Sauvage, 2006). A paracrine mechanism has been implicated in CAFs activation, with Hh ligands secreted by cancer cells activating the glioma-associated transcription factors (Gli) in surrounding stromal cells (Junttila and de Sauvage, 2013; Theunissen and de Sauvage, 2009). Interestingly, while this chain of events should enhance tumor formation (Theunissen and de Sauvage, 2009), an opposite restraining function of stromal Hh-activation in pancreatic and bladder cancer has also been reported (Ozdemir et al., 2014; Rhim et al., 2014; Shin et al., 2014). Mammalian cells express three Gli proteins (Aberger and Ruiz, 2014). Under basal conditions, the Gli2 transcription factor is cleaved into a transcriptional repressor, with Hh stimulation blocking this process and converting it into activator. Expression of the Gli1 transcription factor is then induced, as signal amplifier. In *Drosophila*, the activation of Gli homologue Cubitus Interruptus (Ci) is well established (Ruel et al., 2003; Wang et al., 2000), with a kinase (Fused) releasing it from an inhibitory complex (Costal2/SuFu) and promoting its nuclear translocation. In mammalian cells, the mechanisms responsible for Gli activation are less understood. Recently, the unc-51-like-kinase 3 (Ulk3), an inducer in human fibroblasts of autophagy (Young et al., 2009), has been proposed to fulfill the role of Fused, through association and phosphorylation of Gli2 (Maloverjan et al., 2010; Rubin and de Sauvage, 2006). Importantly, in cancer cells Gli proteins can also be activated by Hh-receptor independent mechanisms involving PI3K/AKT (Metcalfe and de Sauvage, 2011), MAPK/ERK (Seto et al., 2009), S6K (Wang et al., 2012) and KRAS activation (Nolan-Stevaux et al., 2009; Stecca et al., 2007).

Recent evidence suggests that altered metabolic properties of CAFs, resulting from increased autophagy/mitophagy and associated shift to aerobic glycolysis, can contribute to their tumor enhancing properties (Kalluri, 2016; Martinez-Outschoorn et al., 2017). How these processes relate to CAFs activation remains to be determined. We report here a so far

Author Manuscript Author Manuscript Author Manuscript Author Manuscript

unexpected link between the CSL and Gli signaling pathways, with the Ulk3 kinase as an attractive target for stroma-focused anti-cancer intervention, controlling the CAF effectors gene expression program separately from the autophagy/mitophagy processes.

RESULTS

CAF conversion by loss of CSL function depends on Gli activation

The conversion of normal stromal fibroblasts into CAFs is likely to be a multistep process, with loss of CSL transcriptional repression inducing a large battery of CAF effector genes associated with stromal cell senescence, as a fail-safe mechanism limiting cancer/stromal cell expansion (Procopio et al., 2015). An unanswered question is the possible integration of different signaling(s) leading to CAF conversion. Like Notch/CSL, Hh-Gli signaling is deregulated in tumor stroma and can contribute to CAF activation (Junttila and de Sauvage, 2013; Theunissen and de Sauvage, 2009). Under basal conditions, the glioma-associated transcription factor 2 (Gli2) is cleaved into a transcriptional repressor, while block of this process coincides with Gli2 activation and induction of *gli2* and *gli1* expression as signal amplifiers (Aberger and Ruiz, 2014). We found that, in human dermal fibroblasts (HDF), the short repressive form of Gli2 was dramatically reduced, while the full-length transcription-activating protein was induced by 24–48 hours of siRNA-mediated *csl* silencing (Figure 1A), at a time coinciding with induction of CAF effector genes but preceding that of cellular senescence, which occurs only after 4–5 days (Procopio et al., 2015). In parallel, *gli1* and *gli2* expression was up regulated in HDFs and to a similar extent also in human gingival fibroblasts (HGF) (Figures 1B, 1C and S1A).

The above findings are of clinical and functional significance. Patient-derived CAFs have higher Gli2 levels than HDFs, which are inversely related to CSL expression (Figure 1D). Global analysis of gene expression of HDFs vs. CAFs present notable similarities when compared to the expression profile after down modulation of CSL function in HDFs (Procopio et al., 2015), and thus in our studies we focused on a limited-number of CAF genes to characterize the mechanism of HDF conversion to CAF. Functionally, induction of CAF effector genes by *csl* knockdown was blocked in HDFs with concomitant *gli2* silencing (Figure 1E), or in mouse embryo fibroblasts (MEF) with disruption of the *gli1* and *gli2* genes (*gli 1/2* −/−) (Lipinski et al., 2008) (Figures 1F and 1G). Notably, up-regulation of senescent effectors by *csl* loss was unaffected by *gli2* silencing, thus implicating Gli activation selectively in induction of CAF effector genes (Figure S1B and S1C).

An essential property of fibroblasts with deleted or silenced CSL is that they enhance the growth of adjacent cancer cells (Procopio et al., 2015). To test whether these properties are Gli-dependent, we employed a cancer/stromal cell expansion model we developed, based on mouse ear injections of weakly tumorigenic squamous cell carcinoma (SCC) cells admixed with fibroblasts with various genetic manipulations (Procopio et al., 2015). We determined every three days for three weeks the growth of EGFP-expressing SCC13 cells admixed with *gli* +/+ or *gli 1/2* −/− MEFs, both plus/minus *csl* silencing. As previously reported for HDFs with *csl* silencing (Procopio et al., 2015), SCC13 cells admixed with *gli +/+* MEFs with *csl* knockdown formed significantly larger lesions than controls (Figures 1H–1J), while the tumor enhancing effects of *csl* silencing were lost with MEFs with *gli1*/*2* gene deletion

Author Manuscript Author Manuscript Author Manuscript Author Manuscript

(Figures 1H–1J and S1E). Hence our data indicate that CAF conversion of stromal fibroblasts by *csl* loss requires Gli activity.

Ulk3 is a direct CSL target gene, which links *csl* silencing to Gli and CAF activation

In cancer cells, Gli proteins can be activated by Hh-receptor dependent and independent mechanisms (Aberger and Ruiz, 2014). The Ulk3 kinase was recently proposed to fulfill the same role in mammalian cells as the Drosophila Fused in Gli2 activation, through possible association and phosphorylation (Maloverjan et al., 2010; Rubin and de Sauvage, 2006). In agreement with these studies, we confirmed that Ulk3 and Gli2 can be recovered by co-immunoprecipitation in Ulk3-overexpressing cells, in which activated phosphorylated Gli2 (Xing et al., 2014) was detected (Figures 2A and 2B). We also determined the association of endogenous Ulk3 and Gli2 by proximity ligation assays (PLA) in HDFs in which Ulk3 expression was increased by serum starvation (Figures 2C and 2D).

Upon *csl* silencing, levels of *ulk3* expression were significantly induced in several HDFs strains, as well as in HGFs, while expression of two other family members, *ulk1* and *ulk2*, was unaffected (Figures 2E–2G and S2A–S2C). Notably, *ulk3* was also induced after *csl* silencing in MEFs with *gli1/2* gene deletion (Figures 2H and 2I), in which induction of CAF effector genes was blocked (Figures 1F and 1G). Bioinformatic analysis of the 5000bp promoter region of the Ulk3 gene upstream of the initiating ATG revealed the presence of three putative CSL binding sites. Chromatin immunoprecipitation assays (ChIP) of HDFs showed little or no binding of CSL to the first upstream site (Site 1), while the other two were strongly bound, one upstream of the transcription start site (Site2) and the other in the first intron (Site3) (Figure 3J). Histone marks of active chromatin configuration (H3K27ac and H3K4me3) were highly enriched at these sites upon *csl* knockdown (Figures 3K and S2D). Up-regulation of *ulk3* by *csl* silencing is of functional significance, as Gli activation and induction of CAF effector genes were suppressed in cells with concomitant *csl* and *ulk3* knockdown (Figure 3A). Consistent with previous reports (Maloverjan et al., 2010), we found that the activation of Gli reporter activation required Ulk3 kinase activity in HDFs (Figure S2E). In contrast, determinants of cellular senescence (c*dkn1a, cdkna2* and *cdkn2b*) were induced by CSL loss also in concomitance with *ulk3* silencing (Figures S2F and S2G). Conversely, increased *ulk3* expression by lentiviral infection was sufficient to induce *gli* and CAF marker genes (Figures 3B and 3C), with induction of the latter being suppressed in cells with *gli2* silencing (Figure 3D).

An important property of CAFs is the ability to enhance proliferation of neighboring cancer cells. In co-culture assays, proliferation of skin-derived SCC cells (SCC13) was enhanced to a much greater extent by HDFs with silencing of *csl* individually than in combination with *ulk3* (Figures 3E and 3F). Thus, *ulk3* is a direct CSL target gene, which is required for Gli and CAF activation by *csl* down modulation.

CSL silencing and increased Ulk3 induce cellular autophagy and mitophagy separately from Gli and CAF activation

Similarly to other Ulk kinase family members, Ulk3 can plays a key role in initiation of autophagy (Russell et al., 2013; Young et al., 2009). Consistent with the observed up-

Author Manuscript Author Manuscript Author Manuscript Author Manuscript

regulation of *ulk3*, *csl* silencing in HDFs induced autophagy, as assessed by a number of biochemical events, including processing of microtubule-associated protein-1 light chain 3 (LC3) (Klionsky et al., 2016), Beclin-1 phosphorylation (Russell et al., 2013), and down-modulation of the p62 cargo and TOM20 mitochondrial proteins (Bingol et al., 2014; Klionsky et al., 2016) (Figure 4A). Induction of these events was associated with an increase of autophagosome formation, which occurred also in HDFs with *csl* silencing treated with the lysosomal inhibitor Bafilomycin, indicative of an enhanced "on rate" (Figures S3A-S3D). Cellular mitophagy is a selective form of autophagy with a decreased number of mitochondria leading to a metabolic shift towards aerobic glycolysis (Martinez-Outschoorn et al., 2017). After *csl* silencing, both the mitochondrial Tom20 immunofluorescence signal and mitochondrial labelling with MitoTracker were decreased (Figure 4B). Consistent with enhanced mitophagy and glycolytic transition, HDFs with silenced *csl* had enhanced expression of pyruvate kinase isozyme 2 (PKM2) and lactate dehydrogenase A (LDHA), two key enzymes responsible for lactate production (Figure 4C), and higher lactate levels (Figure 4D). A similar induction of autophagy, decreased mitochondria network and increased glycolytic switch were observed in HDFs with increased *ulk3* expression (Figures 4E–4I).

An important question is whether the above processes are linked to induction of the CAF effector gene program or proceed as parallel independent events. Indicative of the second possibility, we found that the silencing of *csl* induced CAF-effector genes to a similar extent in HDFs with or without silencing of the autophagy essential genes *atg5, atg7* or *becn1* (Figure 4J) and in MEFs with *atg5* gene knockout compared to wild type MEFs (Figure S3E). Similarly, increased *ulk3* expression by lentiviral infection induced CAF effector genes in HDFs with silenced *atg5* (Figure 4K). Thus, both *csl* silencing and *ulk3* up-regulation enhance autophagy, which is however dispensable for CAF effectors genes induction.

Ulk3 as a target to suppress CAF activation and cancer/stromal cell expansion

An important question was whether *ulk3* expression is increased also in clinically occurring CAFs. Analysis of published gene expression profiles of CAFs derived from head and neck SCCs (HNSCC) showed that expression of *ulk3* and *gli* is consistently higher than in normal fibroblasts derived from the same body site, with similar up-regulation in CAFs from prostate (Ashida et al., 2012) and breast (Finak et al., 2008) cancers (Figures 5A and S4A).

In skin, laser capture micro-dissection (LCM) followed by RT-qPCR analysis showed consistently increased *ulk3* expression in several SCC-adjacent stromal cells (in areas we tested as devoid of macrophage and leukocyte contamination (Procopio et al., 2015)), relative to stroma areas of distant normal skin (Figure 5B). Results were confirmed by immunofluorescence analysis, showing significantly higher number of Ulk3-expressing fibroblasts (Vimentin positive cells) in SCC surrounding stroma versus unaffected areas of same or different individuals (Figures 5C and S4B). Similarly up-regulated *ulk3* and *gli* levels - with concomitantly decreased *csl* - were also found in CAFs isolated from skin SCCs relative to normal dermal fibroblasts from same or different individuals (Figures 5D–5F and S4C). Results were further validated in a mouse model of AK based on mesenchymal

Author Manuscript Author Manuscript Author Manuscript Author Manuscript

deletion of the *csl* gene (Hu et al., 2012). LCM and RT-qPCR analysis showed significant *ulk3* up regulation in stromal fibroblasts of skin lesions that developed in these mice at 3 months of age, relative to distant unaffected skin (Figure 5G).

To assess whether the observed increase in *ulk3* expression and Gli activation in CAFs is functionally linked to decreased *csl*, we infected these cells with a *csl*-inducible lentivirus, we previously showed to suppress CAF marker expression (Procopio et al., 2015). As shown in Figure 5H increased *csl* expression caused a significant down-regulation of *ulk3* and *gli* levels.

A much-needed development for cancer therapy is the identification of strategies affecting cancer stroma (Goruppi and Dotto, 2013). We found that siRNA-mediated silencing of *ulk3* in two different CAFs strains down-modulated key CAF effector genes and decreased *gli1, gli2* expression (Figure S5A), suggesting that *ulk3* could be an attractive target to counteract CAF activation. We tested this possibility by the same cancer/stromal cell expansion assays employed above, by parallel injections into mouse ears of SCC13 cells admixed with two different strains of patient-derived CAFs plus/minus shRNA-mediated *ulk3* silencing. As shown in Figures 6A and S5B, ear lesions formed in the presence of CAFs with *ulk3* knockdown were consistently smaller than with corresponding CAFs controls. This was paralleled by a lower number of cancer cells positive for the p63 differentiation marker and reduced ki67 proliferative index (Figure 6B). Importantly, key CAF markers, like α-Smooth Muscle Actin (SMA), Periostin (POSTN) and Tenascin C (TNC) were expressed to a much lower extent in lesions with *ulk3*-silenced CAFs than corresponding controls, with increased macrophage infiltration and lesser angiogenesis, as assessed by antibodies against CD68 and CD31 markers, respectively (Figures 6C and S5C). These data indicate that *ulk3*, whose expression is elevated in clinically derived CAFs, is required for the tumor growth-enhancing activity of these cells.

DISCUSSION

Genes with critical cell and tissue regulatory functions are tightly controlled by the convergence of multiple positive and negative signals. While a large number of CAF effector genes have been identified, an unanswered question is the integration of different signaling pathways involved in their control. In stromal fibroblasts, CSL represses senescence- and CAF-effector genes, with induction of the first class of genes occurring as the result of loss of CSL repression and increased p53 activity (Procopio et al., 2015). We show here that relief of CSL repression of CAF effector genes is not sufficient for induction of their expression, for which activation of Gli1/2 transcription factors is also required. Increased expression of the Ulk3 kinase, which occurs in CAFs from various cancer types, provides a link between compromised CSL function and Gli activation, which can occur in concert with other previously reported Hh-receptor dependent and independent mechanisms (Metcalfe and de Sauvage, 2011; Seto et al., 2009); (Wang et al., 2012) (Nolan-Stevaux et al., 2009; Stecca et al., 2007). Autophagy can create a pro-tumorigenic microenvironment rich of metabolic precursors directed from CAFs to tumors (Lisanti et al., 2010; Zhao et al., 2013). As Ulk3 is also an inducer of this process, it provides an attractive target for stroma-focused anti-cancer intervention, to suppress combined aspects of CAF activation.

Author Manuscript Author Manuscript Author Manuscript Author Manuscript

CSL is endowed with an intrinsic transcription repressive function and CAF effector genes are induced as a consequence of CSL down-modulation (Hu et al., 2012; Procopio et al., 2015), as it can occur upon exposure to pro-carcinogenic stimuli such as UVA or smoke-derived compounds (Menietti et al., 2016). We show that loss of CSL transcription repressive function is by itself not sufficient for induction of these genes and for the resulting tumor growth enhancing activity of fibroblasts, for which Gli activation is needed. Aberrant activation of Hh/Gli signaling has been implicated in up to one-third of all human cancers and is considered to be both a consequence and driver of tumor-stromal interactions(Gupta et al., 2010; Ruiz i Altaba et al., 2002). Hh ligands have been implicated as paracrine mediators of cancer development(Rubin and de Sauvage, 2006). Earlier studies indicated that production of these molecules by colon, pancreatic and ovarian cancers cells can promote tumor growth indirectly by activating Hh signaling in surrounding stroma(Theunissen and de Sauvage, 2009). However, recent evidence points to a restraining role of Hh stimulation in pancreatic and bladder cancer stroma (Ozdemir et al., 2014; Rhim et al., 2014; Shin et al., 2014). In our own analysis of multiple HDFs strains plus/minus *csl* silencing and skin-derived CAFs versus matched and unmatched controls, expression of Hh ligands was variously modulated. Similar variations were found in published profiles of CAFs from other cancer types. An attractive possibility is that, irrespectively of Hh levels, Gli activation in stromal fibroblasts can occur through increased activity of the Ulk3 kinase, encoded by a direct CSL target gene up-regulated by *csl* down modulation.

Ulk3 was recently proposed to fulfill the same central role in mammalian cells as the Drosophila Fused kinase in Gli2 activation(Maloverjan et al., 2010). Besides confirming these results, we found a detectable association of endogenous Ulk3-Gli2 in HDFs and showed that increased *ulk3* expression was both required and sufficient for Gli and CAF activation. Separately from this, we uncovered an interplay between CSL and Ulk3 in control of autophagy that may apply, with context-dependent adjustments, to other cellular systems in which Notch signaling has been pharmacologically implicated (Barth and Kohler, 2014; Chen et al., 2016; Song et al., 2015; Yao et al., 2015). Importantly, while autophagy/mitophagy have been previously implicated in metabolic reprogramming of CAFs (Kim et al., 2011; Russell et al., 2013), our genetic evidence indicates that they are not significantly involved in the gene expression program leading to CAF activation.

A much-needed development for cancer therapy is the identification of strategies affecting cancer stroma (Goruppi and Dotto, 2013). As in HDFs with *csl* silencing and CAFs from skin SCCs, analysis of publically available gene expression profiles indicated that *ulk3* expression is elevated in CAFs derived from several different cancer types, including HNSCC, prostate and breast cancer. Functionally, genetic suppression of *ulk3* in patient-derived CAFs was sufficient to inhibit CAF-effector gene expression as well as Gli2 activation, and suppressed the growth-enhancing and pro-tumorigenic properties of these cells on neighboring cancer cells. While similar effects were observed with a compound reported to inhibit Ulk3 kinase activity, further translational studies await the identification of compounds with greater specificity. Thus Ulk3 kinase by linking two key signaling pathways involved in CAF conversion represents an interesting target for stroma-focused anti-cancer interventions.

Author Manuscript Author Manuscript Author Manuscript Author Manuscript

EXPERIMENTAL PROCEDURES

Cell Manipulations

HDFs were prepared from discarded skin samples of abdominoplasty patients at Massachusetts General Hospital (Boston, Massachusetts, USA) with institutional approval (2000P002418) or previously obtained (Procopio et al., 2015). Conditions for culturing cells, viral infection, siRNA-mediated gene silencing, RT–qPCR and ChIP were previously reported (Brooks et al., 2014; Hu et al., 2012). For derivation of CAFs and NFs, surgically excised discarded skin SCC samples and non-affected skin samples, were dissociated with Liberase TL (Roche). For co-culture and *in vivo* approaches, skin SCC13 cells (Restivo et al., 2011) were infected with an EGFP-expressing lentivirus (Tiscornia et al., 2003). Each strain derived from a patient was identified with a number, which is indicated in the different panels. Spontaneously immortalized MEFs plus/minus combined deletion of the *gli1* and *gli 2* genes (Lipinski et al., 2008) were infected with *ulk3* silencing or empty vector control lentiviruses and selected with puromycin. After 2 weeks cells were analyzed by immunofluorescence and for gene expression, then used for the in vivo studies.

Immunofluorescence, autophagy studies and cell assays

Immunoblots and immunofluorescences were performed as in (Kong et al., 2010; Procopio et al., 2015). For immunofluorescence cells were seeded on coverslips, fixed in 3% PFA and processed as in (Kong et al., 2010). Immunohistochemistry of tumor and tissue sections was performed as in (Brooks et al., 2014; Hu et al., 2012; Procopio et al., 2015) and quantification of ki67 and p63 protein levels was made using the watershed algorithm (http://imagej.nih.gov/ij/plugins/watershed.html) and ImageJ, NIH. Quantification of all other tissue immunofluorescence staining was performed using ImageJ.

Autophagosome evaluation studies were performed as in (Kong et al., 2010). Two different strains of HDFs were infected with pHcRed1-LC3 encoding for the far-red fluorescent protein (Clontech) fused to LC3.

Colorimetric determination of lactate was performed using an EnzyChrom L-lactate assay kit (BioAssay Systems). The cell culture supernatants of HDFs with *csl* silencing or overexpressing Ulk3-V5 were collected after three days of culture. Each sample reaction was carried out in triplicate and a standard curve of lactate was used to determine the lactate concentration.

For mitochondrial labeling HDFs plus/minus *csl* silencing for three days were pulse labeled with 100nM MitoTracker Red FM (Thermofisher), fixed with 3% PFA in PBS and analyzed using confocal microscopy (Zeiss Observer Z1) using a Zen Pro 2.3 software. DAPI stained the nuclei.

The siRNA and shRNA sequences used are in TABLES1 and TABLES2. The oligonucleotides used in RT-qPCR are provided in TABLES3. The oligonucleotides used in ChIP experiments are provided in TABLES4. A detailed list of all the antibodies and the condition(s) used is in TABLE S5. Unprocessed original scans of immunoblots are shown in Supplementary Figures S6–S8.

Author Manuscript Author Manuscript Author Manuscript Author Manuscript

Human samples and LCM experiments

Normal human skin samples and samples of squamous cell carcinoma (SCC) were obtained at the Department of Dermatology, Massachusetts General Hospital, as discarded parts not needed for diagnosis. All samples were processed as approved by the Institutional Review Board. Matched normal skin and SCC paraffin samples used for LCM and RT-PCR were provided by the Department of Dermatology, University of Tubingen with institutional review board approvals and informed consent, previously repoted in (Procopio et al., 2015). LCM was made using an Arcturus XT micro-dissection system (Applied Biosystems) as in (Hu et al., 2012; Procopio et al., 2015). Gene expression was normalized to *36β4*, and the absence of contaminating leucocytes in the selected areas was previously confirmed with CD45 oligos in RT-qPCR assays(Procopio et al., 2015).

Animal studies

Experiment with *gli1* and *2* −/− MEFs: Mouse ear injections with the MEFs were carried out in 8 to 10-week-old female SKID (CB17sc-m) mice (Taconic), as in (Procopio et al., 2015). EGFP expressing SCC13 cells (1×10^5) were admixed with equal numbers of MEFs (either *gli* +/+ or *gli 1*/*2* −/−) with shRNA-mediated silencing of *csl*, or a control. Cells were injected 5μl per site using a 33-gauge micro syringe (Hamilton). Starting the day after injection, the mice ears were imaged using a fluorescent stereomicroscope (Leica MZ-FLIII), every three days for 21 days. The mice were sacrificed after 24 days and images of the ears taken using bright field and fluorescence stereomicroscopy. Experiment with patient-derived CAFs: Mouse ear injections of cells were carried out in SKID mice admixing EGFP expressing SCC13 cells (1×10^5) with equal numbers of CAFs (strain#1 or strain#3) infected with an *ulk3* silencing lentivirus or empty vector control. Mice were sacrificed after 3 weeks. All animal studies were approved by MGH institutional animal care and use committee (2004N000170).

Statistical analysis

Data are presented as mean± SEM, mean ± SD, or ratios among treated and controls, with two to three separate HDFs strains in independent experiments as indicated in the Figure legends. For gene expression and functional testing assays, statistical significance of differences between experimental groups and controls was assessed by two-tailed unpaired or paired t-test, and one sample t-test. P values < 0.05 were considered as statistically significant.

Supplementary Material

Refer to Web version on PubMed Central for supplementary material.

Acknowledgments

We are grateful to Robert Lipinski for the MEFs *gli1/2* −/− and *gli +/+* and to Noburo Mitzushima for the MEFs *atg5* −/− and *atg5 +/+*. We thank Liuqing Yang for the P-Gli2 antibodies, Alessia Di Nardo for the *shatg5* vector, Shanell Moijta for technical support with histology and Wolfram Hoetzenecker, for providing SCC samples used in LCM. A. C. is supported by a Marie Curie fellowship from the Italian Association for Cancer Research and the European Union FP7 Marie Curie Program. This work was supported by grants from the National Institutes of Health (R01AR039190; R01AR064786; the content not necessarily representing the official views of NIH), the

Swiss National Science Foundation (310030_156191/1) and European Research Council (26075083) to GPD. The Authors declare that there are no competing financial interests.

References

Aberger F, Ruiz IAA. Context-dependent signal integration by the GLI code: the oncogenic load, pathways, modifiers and implications for cancer therapy. Semin Cell Dev Biol. 2014; 33:93–104. [PubMed: 24852887]

Allenspach EJ, Maillard I, Aster JC, Pear WS. Notch signaling in cancer. Cancer Biol Ther. 2002; 1:466–476. [PubMed: 12496471]

Artavanis-Tsakonas S, Rand MD, Lake RJ. Notch signaling: cell fate control and signal integration in development. Science. 1999; 284:770–776. [PubMed: 10221902]

Ashida S, Orloff MS, Bebek G, Zhang L, Zheng P, Peehl DM, Eng C. Integrated analysis reveals critical genomic regions in prostate tumor microenvironment associated with clinicopathologic phenotypes. Clin Cancer Res. 2012; 18:1578–1587. [PubMed: 22275508]

Barth JM, Kohler K. How to take autophagy and endocytosis up a notch. BioMed research international. 2014; 2014:960803. [PubMed: 24860831]

Bingol B, Tea JS, Phu L, Reichelt M, Bakalarski CE, Song Q, Foreman O, Kirkpatrick DS, Sheng M. The mitochondrial deubiquitinase USP30 opposes parkin-mediated mitophagy. Nature. 2014; 510:370–375. [PubMed: 24896179]

Bissell MJ, Hines WC. Why don't we get more cancer? A proposed role of the microenvironment in restraining cancer progression. Nat Med. 2011; 17:320–329. [PubMed: 21383745]

Brooks YS, Ostano P, Jo SH, Dai J, Getsios S, Dziunycz P, Hofbauer GF, Cerveny K, Chiorino G, Lefort K, et al. Multifactorial ERbeta and NOTCH1 control of squamous differentiation and cancer. J Clin Invest. 2014; 124:2260–2276. [PubMed: 24743148]

Chen X, Zhang Y, Shi Y, Lian H, Tu H, Han S, Yin J, Peng B, Zhou B, He X, et al. MiR-129 triggers autophagic flux by regulating a novel Notch-1/E2F7/Beclin-1 axis to impair the viability of human malignant glioma cells. Oncotarget. 2016; 7:9222–9235. [PubMed: 26824182]

Costea DE, Hills A, Osman AH, Thurlow J, Kalna G, Huang X, Pena Murillo C, Parajuli H, Suliman S, Kulasekara KK, et al. Identification of two distinct carcinoma-associated fibroblast subtypes with differential tumor-promoting abilities in oral squamous cell carcinoma. Cancer Res. 2013; 73:3888–3901. [PubMed: 23598279]

Dotto GP. Notch tumor suppressor function. Oncogene. 2008; 27:5115–5123. [PubMed: 18758480]

Dotto GP. Crosstalk of Notch with p53 and p63 in cancer growth control. Nat Rev Cancer. 2009; 9:587–595. [PubMed: 19609265]

Dotto GP. Multifocal epithelial tumors and field cancerization: stroma as a primary determinant. J Clin Invest. 2014; 124:1446–1453. [PubMed: 24691479]

Finak G, Bertos N, Pepin F, Sadekova S, Souleimanova M, Zhao H, Chen H, Omeroglu G, Meterissian S, Omeroglu A, et al. Stromal gene expression predicts clinical outcome in breast cancer. Nat Med. 2008; 14:518–527. [PubMed: 18438415]

Goruppi S, Dotto GP. Mesenchymal stroma: primary determinant and therapeutic target for epithelial cancer. Trends Cell Biol. 2013

Gupta S, Takebe N, LoRusso P. Targeting the Hedgehog pathway in cancer. Therapeutic Advances in Medical Oncology. 2010; 2:237–250. [PubMed: 21789137]

Hanahan D, Weinberg RA. Hallmarks of cancer: the next generation. Cell. 2011; 144:646–674. [PubMed: 21376230]

Hu B, Castillo E, Harewood L, Ostano P, Reymond A, Dummer R, Raffoul W, Hoetzenecker W, Hofbauer GF, Dotto GP. Multifocal epithelial tumors and field cancerization from loss of mesenchymal CSL signaling. Cell. 2012; 149:1207–1220. [PubMed: 22682244]

Junttila MR, de Sauvage FJ. Influence of tumour micro-environment heterogeneity on therapeutic response. Nature. 2013; 501:346–354. [PubMed: 24048067]

Kalluri R. The biology and function of fibroblasts in cancer. Nat Rev Cancer. 2016; 16:582–598. [PubMed: 27550820]

Author Manuscript Author Manuscript Author Manuscript Author Manuscript

Author Manuscript Author Manuscript Author Manuscript Author Manuscript

Kim J, Kundu M, Viollet B, Guan KL. AMPK and mTOR regulate autophagy through direct phosphorylation of Ulk1. Nat Cell Biol. 2011; 13:132–141. [PubMed: 21258367]

Klionsky DJ, Abdelmohsen K, Abe A, Abedin MJ, Abeliovich H, Acevedo Arozena A, Adachi H, Adams CM, Adams PD, Adeli K, et al. Guidelines for the use and interpretation of assays for monitoring autophagy (3rd edition). Autophagy. 2016; 12:1–222. [PubMed: 26799652]

Kong DK, Georgescu SP, Cano C, Aronovitz MJ, Iovanna JL, Patten RD, Kyriakis JM, Goruppi S. Deficiency of the transcriptional regulator p8 results in increased autophagy and apoptosis, and causes impaired heart function. Mol Biol Cell. 2010; 21:1335–1349. [PubMed: 20181828]

Lipinski RJ, Bijlsma MF, Gipp JJ, Podhaizer DJ, Bushman W. Establishment and characterization of immortalized Gli-null mouse embryonic fibroblast cell lines. BMC Cell Biology. 2008; 9:49–49. [PubMed: 18789160]

Lisanti MP, Martinez-Outschoorn UE, Chiavarina B, Pavlides S, Whitaker-Menezes D, Tsirigos A, Witkiewicz A, Lin Z, Balliet R, Howell A, et al. Understanding the “lethal” drivers of tumor-stroma co-evolution: emerging role(s) for hypoxia, oxidative stress and autophagy/mitophagy in the tumor micro-environment. Cancer Biol Ther. 2010; 10:537–542. [PubMed: 20861671]

Maloverjan A, Piirsoo M, Michelson P, Kogerman P, Osterlund T. Identification of a novel serine/threonine kinase ULK3 as a positive regulator of Hedgehog pathway. Exp Cell Res. 2010; 316:627–637. [PubMed: 19878745]

Martincorena I, Roshan A, Gerstung M, Ellis P, Van Loo P, McLaren S, Wedge DC, Fullam A, Alexandrov LB, Tubio JM, et al. Tumor evolution. High burden and pervasive positive selection of somatic mutations in normal human skin. Science. 2015; 348:880–886. [PubMed: 25999502]

Martinez-Outschoorn UE, Peiris-Pages M, Pestell RG, Sotgia F, Lisanti MP. Cancer metabolism: a therapeutic perspective. Nat Rev Clin Oncol. 2017; 14:11–31. [PubMed: 27141887]

Menietti E, Xu X, Ostano P, Joseph JM, Lefort K, Dotto GP. Negative control of CSL gene transcription by stress/DNA damage response and p53. Cell Cycle. 2016; 15:1767–1778. [PubMed: 27163456]

Metcalfe C, de Sauvage FJ. Hedgehog fights back: mechanisms of acquired resistance against Smoothened antagonists. Cancer Res. 2011; 71:5057–5061. [PubMed: 21771911]

Nolan-Stevaux O, Lau J, Truitt ML, Chu GC, Hebrok M, Fernandez-Zapico ME, Hanahan D. GLI1 is regulated through Smoothened-independent mechanisms in neoplastic pancreatic ducts and mediates PDAC cell survival and transformation. Genes Dev. 2009; 23:24–36. [PubMed: 19136624]

Ozdemir BC, Pentcheva-Hoang T, Carstens JL, Zheng X, Wu CC, Simpson TR, Laklai H, Sugimoto H, Kahlert C, Novitskiy SV, et al. Depletion of carcinoma-associated fibroblasts and fibrosis induces immunosuppression and accelerates pancreas cancer with reduced survival. Cancer Cell. 2014; 25:719–734. [PubMed: 24856586]

Procopio MG, Laszlo C, Al Labban D, Kim DE, Bordignon P, Jo SH, Goruppi S, Menietti E, Ostano P, Ala U, et al. Combined CSL and p53 downregulation promotes cancer-associated fibroblast activation. Nat Cell Biol. 2015; 17:1193–1204. [PubMed: 26302407]

Restivo G, Nguyen BC, Dziunycz P, Ristorcelli E, Ryan RJ, Ozuysal OY, Di Piazza M, Radtke F, Dixon MJ, Hofbauer GF, et al. IRF6 is a mediator of Notch pro-differentiation and tumour suppressive function in keratinocytes. EMBO J. 2011; 30:4571–4585. [PubMed: 21909072]

Rhim AD, Oberstein PE, Thomas DH, Mirek ET, Palermo CF, Sastra SA, Dekleva EN, Saunders T, Becerra CP, Tattersall IW, et al. Stromal elements act to restrain, rather than support, pancreatic ductal adenocarcinoma. Cancer Cell. 2014; 25:735–747. [PubMed: 24856585]

Rubin LL, de Sauvage FJ. Targeting the Hedgehog pathway in cancer. Nat Rev Drug Discov. 2006; 5:1026–1033. [PubMed: 17139287]

Ruel L, Rodriguez R, Gallet A, Lavenant-Staccini L, Therond PP. Stability and association of Smoothened, Costal2 and Fused with Cubitus interruptus are regulated by Hedgehog. Nat Cell Biol. 2003; 5:907–913. [PubMed: 14523402]

Ruiz i Altaba A, Sanchez P, Dahmane N. Gli and hedgehog in cancer: tumours, embryos and stem cells. Nat Rev Cancer. 2002; 2:361–372. [PubMed: 12044012]

Author Manuscript Author Manuscript Author Manuscript Author Manuscript

Russell RC, Tian Y, Yuan H, Park HW, Chang YY, Kim J, Kim H, Neufeld TP, Dillin A, Guan KL. ULK1 induces autophagy by phosphorylating Beclin-1 and activating VPS34 lipid kinase. Nat Cell Biol. 2013; 15:741–750. [PubMed: 23685627]

Seto M, Ohta M, Asaoka Y, Ikenoue T, Tada M, Miyabayashi K, Mohri D, Tanaka Y, Ijichi H, Tateishi K, et al. Regulation of the hedgehog signaling by the mitogen-activated protein kinase cascade in gastric cancer. Mol Carcinog. 2009; 48:703–712. [PubMed: 19142899]

Shin K, Lim A, Zhao C, Sahoo D, Pan Y, Spiekerkoetter E, Liao JC, Beachy PA. Hedgehog signaling restrains bladder cancer progression by eliciting stromal production of urothelial differentiation factors. Cancer Cell. 2014; 26:521–533. [PubMed: 25314078]

Song BQ, Chi Y, Li X, Du WJ, Han ZB, Tian JJ, Li JJ, Chen F, Wu HH, Han LX, et al. Inhibition of Notch Signaling Promotes the Adipogenic Differentiation of Mesenchymal Stem Cells Through Autophagy Activation and PTEN-PI3K/AKT/mTOR Pathway. Cellular physiology and biochemistry: international journal of experimental cellular physiology, biochemistry, and pharmacology. 2015; 36:1991–2002.

Stecca B, Mas C, Clement V, Zbinden M, Correa R, Piguet V, Beermann F, Ruiz IAA. Melanomas require HEDGEHOG-GLI signaling regulated by interactions between GLI1 and the RAS-MEK/AKT pathways. Proc Natl Acad Sci U S A. 2007; 104:5895–5900. [PubMed: 17392427]

Theunissen JW, de Sauvage FJ. Paracrine Hedgehog signaling in cancer. Cancer Res. 2009; 69:6007–6010. [PubMed: 19638582]

Tiscornia G, Singer O, Ikawa M, Verma IM. A general method for gene knockdown in mice by using lentiviral vectors expressing small interfering RNA. Proc Natl Acad Sci U S A. 2003; 100:1844–1848. [PubMed: 12552109]

Wang G, Amanai K, Wang B, Jiang J. Interactions with Costal2 and suppressor of fused regulate nuclear translocation and activity of cubitus interruptus. Genes Dev. 2000; 14:2893–2905. [PubMed: 11090136]

Wang Y, Ding Q, Yen CJ, Xia W, Izzo JG, Lang JY, Li CW, Hsu JL, Miller SA, Wang X, et al. The crosstalk of mTOR/S6K1 and Hedgehog pathways. Cancer Cell. 2012; 21:374–387. [PubMed: 22439934]

Xing Z, Lin A, Li C, Liang K, Wang S, Liu Y, Park PK, Qin L, Wei Y, Hawke DH, et al. lncRNA directs cooperative epigenetic regulation downstream of chemokine signals. Cell. 2014; 159:1110–1125. [PubMed: 25416949]

Yao J, Zheng K, Li C, Liu H, Shan X. Interference of Notch1 inhibits the growth of glioma cancer cells by inducing cell autophagy and down-regulation of Notch1-Hes-1 signaling pathway. Medical oncology (Northwood, London, England). 2015; 32:610.

Young AR, Narita M, Ferreira M, Kirschner K, Sadaie M, Darot JF, Tavare S, Arakawa S, Shimizu S, Watt FM, et al. Autophagy mediates the mitotic senescence transition. Genes Dev. 2009; 23:798–803. [PubMed: 19279323]

Zhao X, He Y, Chen H. Autophagic tumor stroma: mechanisms and roles in tumor growth and progression. Int J Cancer. 2013; 132:1–8. [PubMed: 22684793]

Author Manuscript Author Manuscript Author Manuscript Author Manuscript

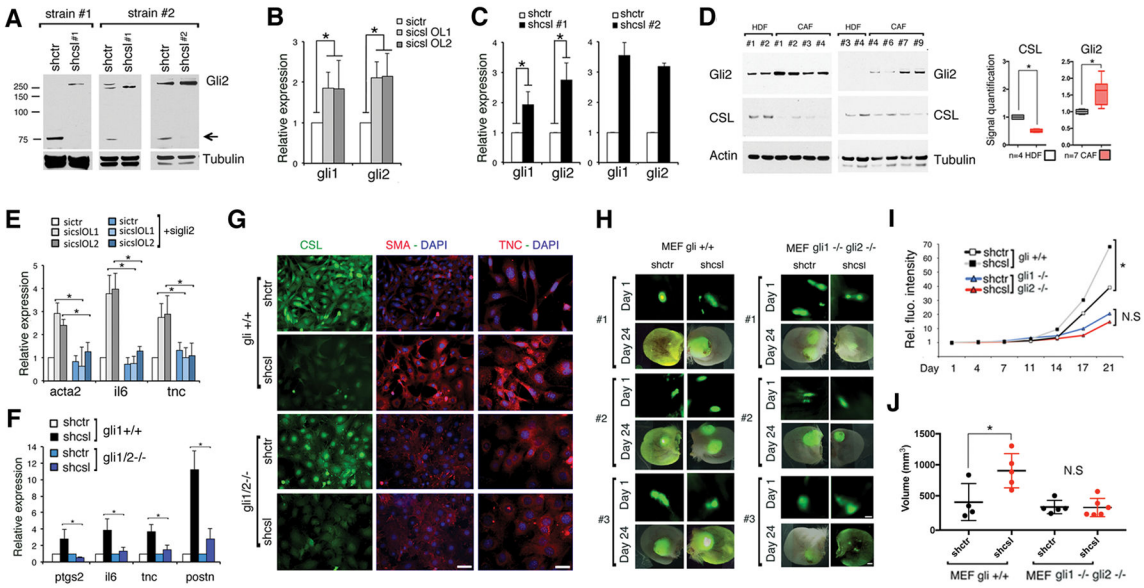

Figure 1. CAF activation by CSL silencing depends on Gli activation

(A) Immunoblot analysis of two HDFs strains plus/minus shRNA-mediated *csl* silencing for 7 days with anti-Gli2 and γ-tubulin antibodies. The arrow points to the truncated Gli2 repressor form.

(B, C) RT-qPCR analysis of *gli1* and *gli2* expression in HDFs, plus/minus siRNA- or shRNA-mediated *csl* silencing. mean±SEM, three HDFs strains, n(experiments)=5 for sicslOL1/2; n(experiments)=3 for shcsl#1; n(experiments)=2, in two HDFs strains for shcsl#2 *p<0.05, two-tailed unpaired t-test. mean±SD. Analysis of HGFs plus/minus *csl* silencing is in Figure S1A.

(D) Left: immunoblots with antibodies against indicated proteins of HDFs and CAFs. Right: immunoblot quantifications, mean±SEM; n(HDF)=4; n(CAF)=7, *p<0.05, two-tailed unpaired t-test.

(E) RT-qPCR analysis of the indicated genes in HDFs plus− *csl* and *gli2* silencing as indicated. Mean±SEM with two HDFs strains, n(experiments)=3, *p<0.05, two-tailed unpaired t-test. Immunoblot analysis verifying *csl* and *gli2* silencing is in Figure S1C

(F) RT-qPCR analysis of the indicated genes in mouse embryo fibroblasts (MEF) with *gli1* and *gli2* gene disruption (*gli 1/2 −/−)*(Lipinski et al., 2008) versus wild type control (*gli +/+)*, stably infected with a *csl* silencing versus control lentiviruses for two weeks. mean ±SEM, n(experiments)=3, *p<0.05, two-tailed unpaired t-test.

(G) Immunofluorescence analysis of *gli +/+* versus *gli 1/2 −/−* MEFs plus/minus shRNA-mediated *csl* silencing as in (F) with the indicated antibodies, and DAPI for nuclear staining. Scale bar 60μM for CSL and SMA; 30μM for TNC.

(H–J) EGFP-expressing SCC13 cells were admixed with either *gli +/+* or *gli 1/2 −/−* MEFs, stably infected with an *csl* silencing or control lentiviruses, followed by parallel injections into contralateral ears of SKID mice. **(H)** Images of combined bright field and fluorescence microscopy of three mice per combination of cells, at day 1 and 21 after injection. **(I)** Increase of average fluorescence signals over time for all tumors per group. Quantification was achieved using ImageJ on images acquired every three days for 21 days as in (Procopio

Author Manuscript Author Manuscript Author Manuscript Author Manuscript

et al., 2015) and normalized to day1 after injection. n(tumors *gli +/+*)= 4 for *shctr* and 5 for *shcsl*; n(tumors *gli 1/2 −/−*)= 5 for *shctr* and 6 for *shcsl*. For *gli 1/2 +/+* MEF *shctr* vs *shcsl* *p<0.05; for *gli1/2 −/−* MEF *shctr* vs *shcsl* NS = not significant, two-tailed equal variance unpaired t-test. **(J)** Tumor volumes, measured as (V= (length × width^2)*.5), after 24 days from injection of admixed cells indicated in panel I. Median and SD are indicated. For *gli +/+* MEFs *shctr* vs *shcsl,* *p=0.0091 and for *gli1/2 −/−* MEFs *shctr* vs *shcsl*, p=NS (not significant), unpaired samples, two-tailed equal variance t-test. Scale bar, 30μm for Day 1 and 5 mm for Day 21. The quantification comparing the lesions *(shcsl/shctr)* formed in the same animal is in Figure S1D. See also Figure S1.

Author Manuscript Author Manuscript Author Manuscript Author Manuscript

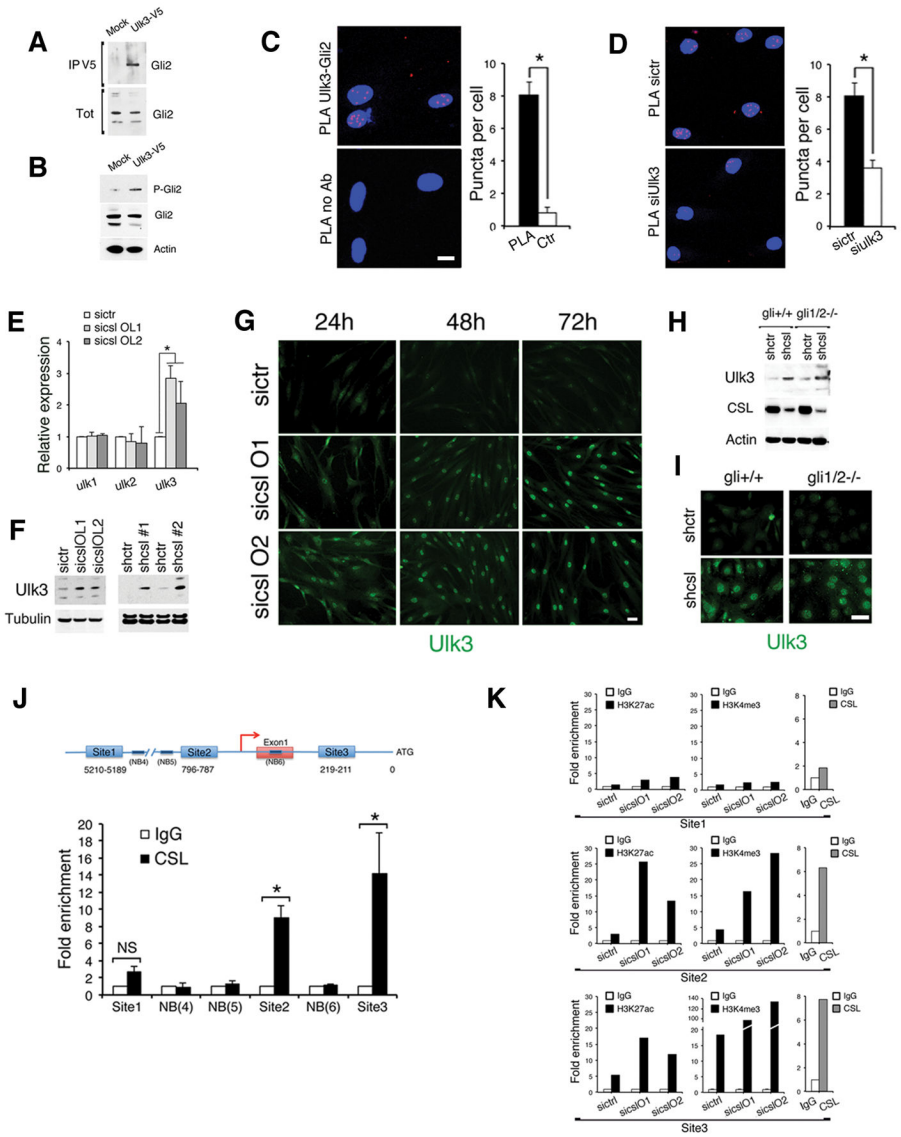

Figure 2. Ulk3 is a direct CSL target gene which links *csl* silencing to Gli activation

(A) Immunoblot with anti-Gli2 antibodies of HEK293 cells transfected with an Ulk3-V5 tag expressing versus empty vector control (Mock) after immunoprecipitation with anti-V5 antibodies with total input (Tot) as loading control.

(B) Immunoblot of total HEK293 extracts after transfection as in (A) with antibodies against activated phospho-Gli2 (Ser149) (Xing et al., 2014), Gli2 and β-actin.

(C–D) Proximity ligation assays (PLA) with antibodies against Ulk3 and Gli2 of HDFs serum starved for 24 hours for up regulation of endogenous Ulk3. Assays without primary antibodies (no Ab) (C) or with cells with siRNA-mediated *ulk3* silencing (D) were used for specificity controls. Red fluorescence *puncta* resulting from juxtaposition of anti-Ulk3 and -Gli2 antibodies were visualized by confocal microscopy with DAPI nuclear staining. Number of *puncta* per cell, n(cells)>120 per condition $p<0.05$, two-tailed unpaired t-test.

Author Manuscript Author Manuscript Author Manuscript Author Manuscript

(E) RT-qPCR analysis of *ulk1-3* expression in HDFs plus/minus siRNA-mediated *csl* silencing with *β-actin* normalization. mean±SEM n(experiments)=5, three HDFs strains, *p<0.05, two-tailed unpaired t-test. RT-qPCR analysis of HDFs and human gingival fibroblasts (HGFs) plus/minus shRNA-mediated *csl* silencing are in Figures S2A and S2B.
(F) Immunoblot analysis of HDFs plus/minus siRNA- and shRNA- mediated *csl* silencing with antibodies against Ulk3 and γ-tubulin. Immunoblot analysis of HGFs plus/minus *csl* silencing is in Figure S2C.
(G) Immunofluorescence analysis of HDFs at various times (hours) from siRNA-mediated *csl* silencing with antibodies against Ulk3. Bar 30 μm.
(H) Immunoblot analysis of *gli +/+* versus *gli1/2 −/−* MEFs plus/minus shRNA-mediated *csl* silencing with antibodies against Ulk3 and β-Actin.
(I) Immunofluorescence with anti-Ulk3 antibodies of MEFs as in (H), Bar 30μm.
(J) Upper: scheme of the human *ulk3* gene around the transcription start site (red arrow) and first non-coding exon with nucleotide position of predicted CSL binding sites (Site1,2,3,) relative to the initiation codon (ATG) and non-binding regions (NB4,5,6). Lower: Chromatin immunoprecipitation assays of HDFs with anti-CSL (CSL) or non-immune antibodies (IgG) followed by binding determination of the indicated regions of the *ulk3* gene by qPCR. Results are expressed as enrichment fold relative to input, mean±SEM, using two HDFs strains, n(experiments)=3; *p<0.05 and NS=not significant, two-tailed unpaired t-test.
(K) Chromatin immunoprecipitation assays ChIP at the CSL binding sites in of HDFs plus/minus *csl* silencing with antibodies against active histone marks (H3K27Ac27 and H3K4me3) versus non-immune IgG (black and white bars, respectively) for the CSL binding sites at the *ulk3* promoter region. Parallel chromatin immunoprecipitation assays with anti-CSL antibodies of HDFs are shown (grey and white bars). Results obtained using a different HDF strain in Figure S2D. See also Figure S2.

Author Manuscript Author Manuscript Author Manuscript Author Manuscript

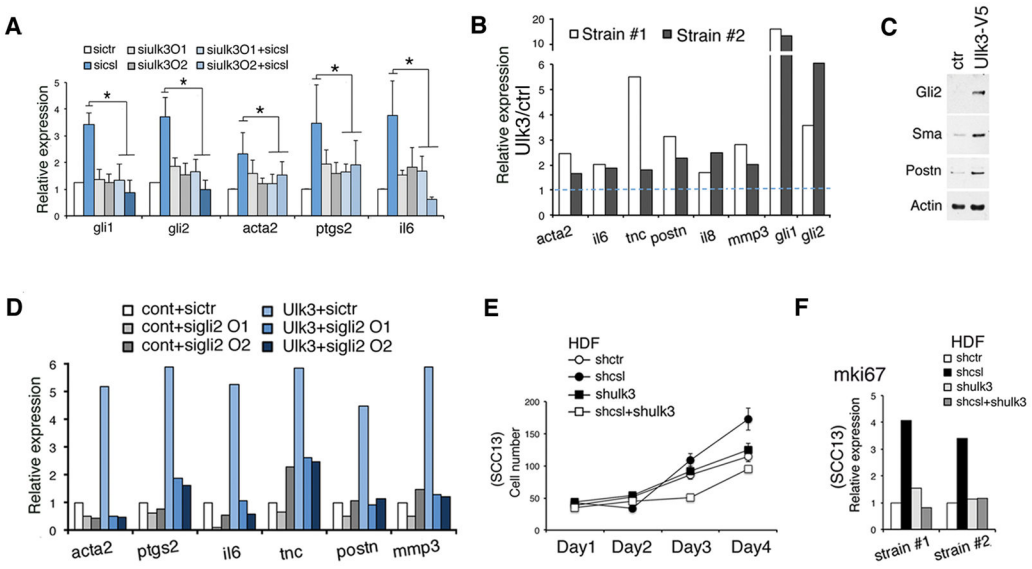

Figure 3. Ulk3 activity is required for induction of Gli1/2 and CAF effectors by *csl* silencing

(A) RT-qPCR analysis of the indicated genes in HDFs plus/minus *csl* and *ulk3* silencing individually and in combination. mean±SEM with two HDFs strains, n(experiments)=3, *p<0.05, two-tailed unpaired t-test. An immunoblot analysis verifying *csl* and *ulk3* silencing is shown in Figure S2G.

(B) RT-qPCR of the indicated genes in HDFs infected with *ulk3*-expressing versus empty vector control lentiviruses. Results are expressed as folds of expression over control, after *β-actin* normalization. n(strains)=2.

(C) Immunoblot of HDFs infected with same viruses as in (B) with antibodies against the indicated proteins.

(D) RT-qPCR of the indicated genes in HDFs infected with an Ulk3-expressing (Ulk3) versus control (cont) virus for one week, then plus/minus *gli2* silencing for 48 hours (total 9 days). Results are expressed as folds of expression in Ulk3 overexpressing versus control.

(E) Cell counts of EGFP- SCC13 cells cultured for 4 days on well inserts with HDFs plus/minus *csl* and/or *ulk3* silencing in the bottom. Duplicate cultures were photographed daily and number of EGFP-SCC13 cells were quantified using ImageJ software. mean±SD

(F) RT-qPCR analysis of *mki67* expression, normalized to *β-actin,* in SCC13 cells co-cultured for 4 days with two different HDFs strains plus/minus *csl* and *ulk3* silencing as in (E). n(strains)=2.

Author Manuscript Author Manuscript Author Manuscript Author Manuscript

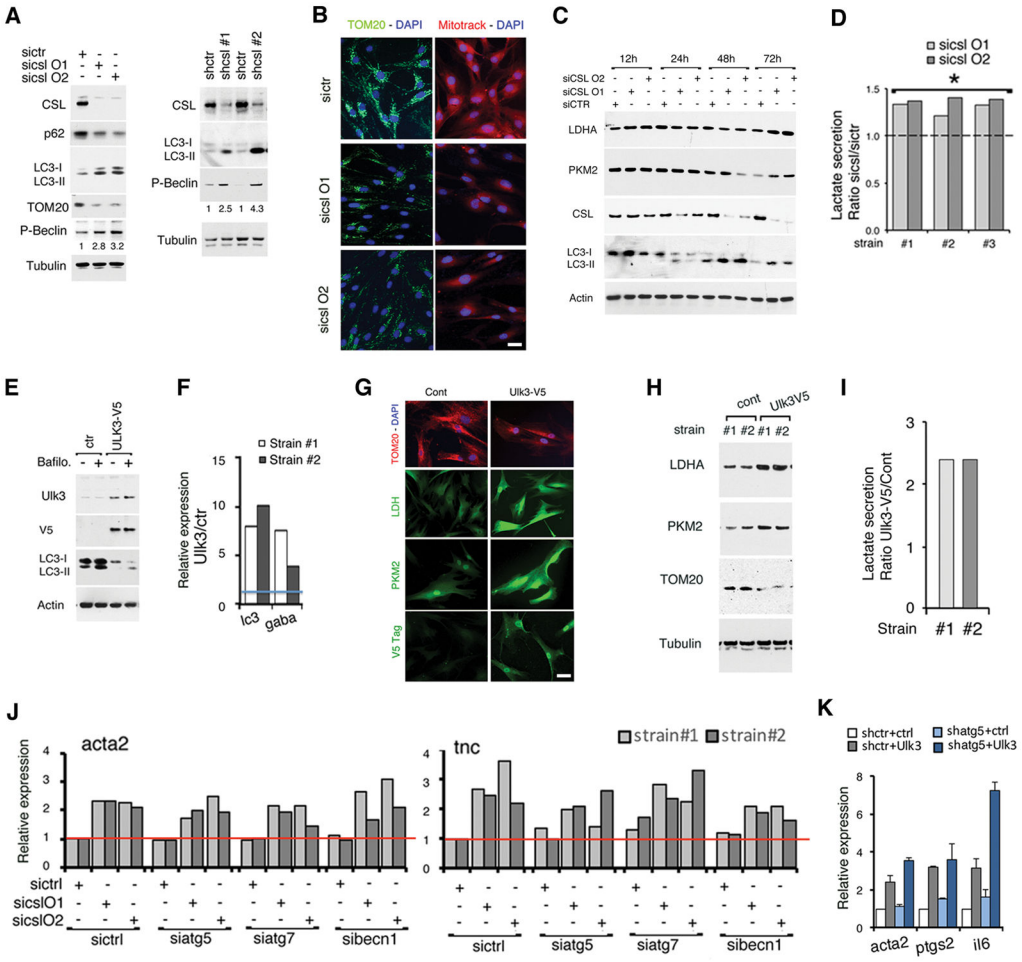

Figure 4. *Csl* silencing and increased Ulk3 induce cellular autophagy and mitophagy separately from Gli and CAF activation

(A) Immunoblot analysis with antibodies against indicated proteins of HDFs plus/minus *csl* silencing with siRNAs for 48 hours (left panel) or shRNAs for one week (right panel). Numbers refer to densitometric quantification (folds of induction) of phospho-Beclin1 in *csl*-silenced versus control cells. Immunofluorescent analysis of endogenous puncta formation plus/minus si*csl* and of Red fluorescent protein expressing HDFs plus minus si*csl* and +/− Bafilomycin are in Figures S3A-S3C. Western blot of LC3-processing plus minus si*csl* and +/− Bafilomycin is in Figure S3D.

(B) Immunofluorescence analysis with anti-TOM20 antibodies or MitoTracker Deep Red FM staining (right and Ieft panels, respectively) of HDFs plus/minus *csl* silencing with siRNAs for three days. Bar 10μm.

(C) Immunoblot analysis of HDFs plus/minus *csl* silencing with siRNAs for three days using antibodies against indicated proteins.

(D) Lactate secretion in culture medium of three HDFs strains plus/minus siRNA *csl* silencing for three days. Results are expressed as ratio *sicsl/sictr*, normalized for cell numbers. n(strains)=3; *p<0.05, one sample t-test.

Author Manuscript Author Manuscript Author Manuscript Author Manuscript

(E) Immunoblot with antibodies against indicated proteins of HDFs infected with Ulk3-V5-expressing versus control viruses (7 days) plus/minus Bafilomycin (400nM) (last 4 hours of the experiment).

(F) RT-qPCR of the indicated genes in two HDFs strains infected with Ulk3-V5-expressing versus control viruses. Results are expressed as relative folds of expression over control, n(strains)=2.

(G) Immunofluorescence analysis of HDFs infected with Ulk3-V5 expressing versus control viruses, using antibodies against TOM20, LDH, PKM2 and V5-tag. Bar 30μm.

(H) Immunoblot analysis of HDFs infected as in previous panel with antibodies against indicated proteins. n(strain)=2.

(I) Lactate secretion in culture medium of two independent HDFs strains infected with Ulk3-V5 expressing versus control viruses for 7 days. Results are expressed as ratio over control, after cell number normalization. n(strains)=3; *$p<0.05$, one sample t-test..

(J) RT-PCR analysis of α-SMA (*acta2*) and tenascin (*tnc*) genes in HDF plus/minus siRNA-mediated silencing of *csl* individually and in combination with *atg5*, *atg7* or *becn1*, as indicated. n(strain)=2. RT-PCR analysis of CAF effector genes up regulation after *csl* shRNA in MEF *+/+* and *−/− atg5* s is in Figure 3E.

(K) RT-qPCR of the indicated genes in HDFs infected with an *atg5*-silencing virus versus control for 7 days, and subsequent infection with an Ulk3-V5-overexpressing and corresponding control viruses for 3 additional days (total 10 days). Folds of expression over control, mean±SD, n(strain)=2. See also Figure S3.

Author Manuscript Author Manuscript Author Manuscript Author Manuscript

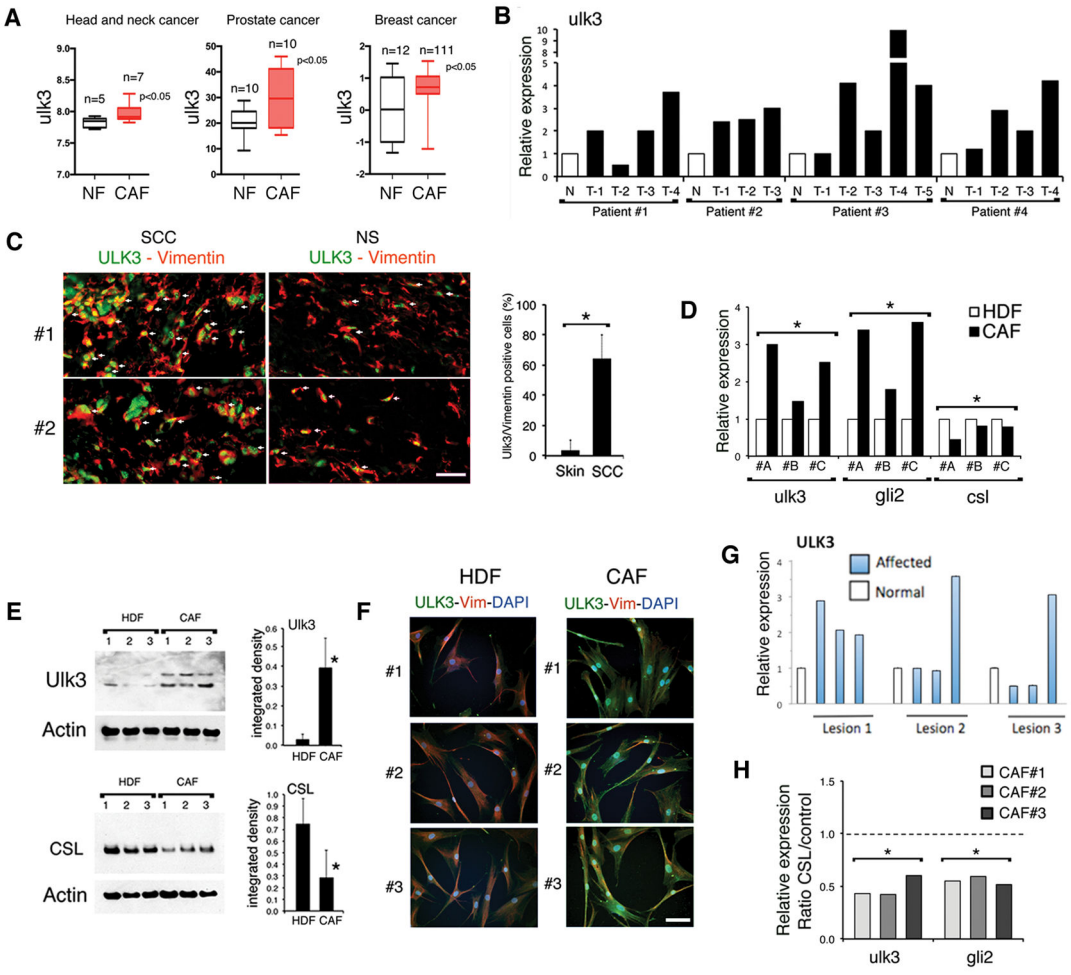

Figure 5. Ulk3 levels are elevated in CAFs

(A) *Ulk3* levels in published gene expression profiles of CAFs derived from head/neck SCC (Costea et al., 2013), prostate (Ashida et al., 2012) and breast (Finak et al., 2008) cancer; head/neck n=7 CAFs and n=5 healthy individuals; prostate n=10 CAFs and n=10 healthy patients; Breast n=111 CAFs and n=12 healthy patients; two class comparison t-tests *<0.05, NFs vs CAFs. Median, max and min (vertical whiskers) are represented. The levels of *gli1* and *gli2* expression in these gene sets are in Figure S4A.

(B) Laser capture micro-dissection (LCM) and RT-qPCR analysis of *ulk3* expression, normalized to *36β4*, of stromal cells surrounding SCC versus normal skin from the same patient (n=4). The captured stromal cells in the SCC areas, indicated as T1-5, were previously characterized as negative for macrophage and leukocyte infiltration and down-modulated *csl* expression(Procopio et al., 2015).

(C) Left: Double immunofluorescence analysis of stromal areas of two patient-derived squamous cell carcinomas (SCC) and normal skin (NS) from the same individuals using anti-Vimentin (Red) and anti-Ulk3 (green) antibodies. Arrows point to cells double positive for Vimentin and Ulk3. Bar 100μm. Additional images of SCCs and NSs are in Figure S4B. Right: quantification of Vimentin-positive cells also Ulk3-positive in stroma of 4 NSs donors compared to 4 matched and additional 6 unmatched SCCs patients. At least 100 cells were

Author Manuscript Author Manuscript Author Manuscript Author Manuscript

counted for each sample, n(sample)=10 for SCCs and n(sample)=4 for NSs, *p<0.05, two-tailed unpaired t-test.

(D) RT-qPCR analysis of the indicated genes in SCC-derived CAFs versus matched normal HDFs from the same patients. n(patient)=3, *p<0,05, two-tailed unpaired t-test.

(E) Left: immunoblotting with antibodies against Ulk3, CSL and β-actin of CAFs and HDFs from different individuals. Right: Densitometric quantification, mean±SEM n(strain)=3; *p<0,05, two-tailed unpaired t-test. Immunoblot of additional four CAFs and two HDFs strains in Figure S4C.

(F) Immunofluorescence analysis of CAFs and HDFs strains as in (E) with antibodies against Ulk3 (green), vimentin (red) and DAPI staining (blue). Bar 30μm.

(G) RT-PCR analysis of *ulk3* expression in three LCM-obtained normal and affected stromal areas in the skin of 3 months old mice having the CSL gene deleted. Samples were previously characterized for other genes in (Procopio et al., 2015). n(lesions)=3.

(H) RT-qPCR analysis of the indicated genes, with 36*β4* for normalization, in same CAFs strains as in (E) stably infected with a doxycycline-inducible *csl* expression or an empty vector virus and plus/minus doxycycline for 3 days. n(CAF)=3, *p<0.05, one sample t-test. See also Figure S4.

Author Manuscript Author Manuscript Author Manuscript Author Manuscript

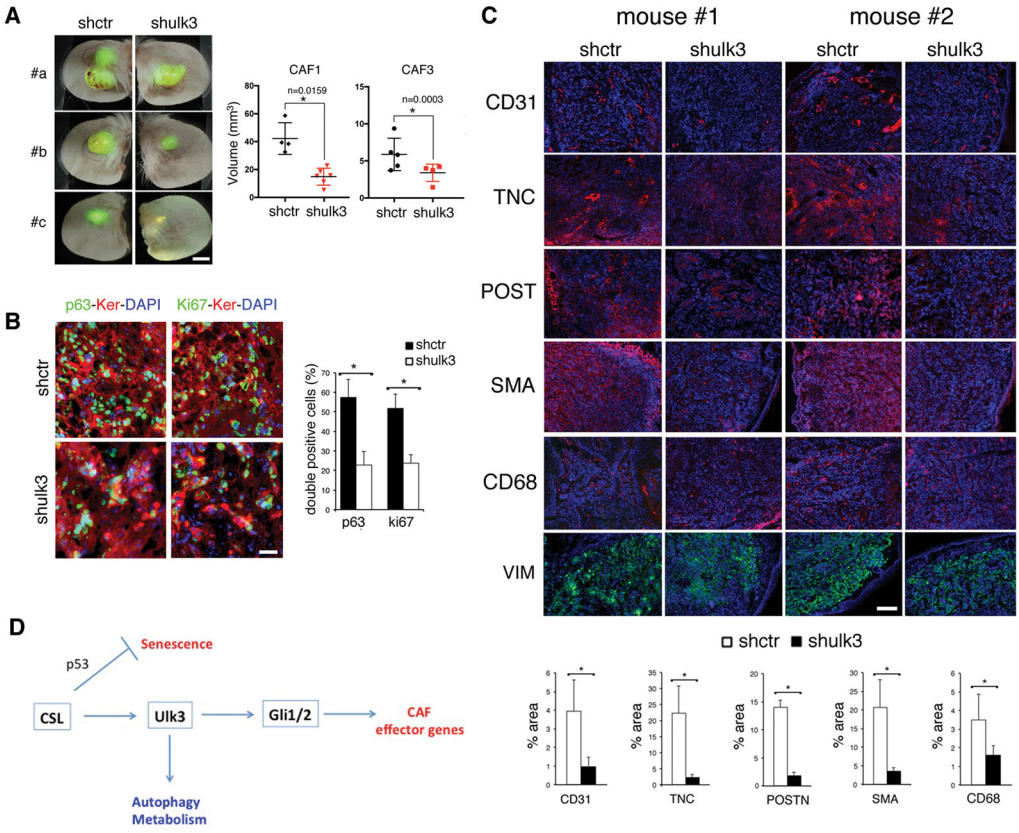

Figure 6. Loss of Ulk3 suppresses CAFs tumor-enhancing properties

(A) EGFP-expressing SCC13 cells admixed with two different CAFs strains (CAF #1 and #3) infected with an *ulk3*-silencing versus control lentiviruses were injected into contralateral ears of SKID mice. Left: representative bright field and fluorescence images of three mouse ear pairs (#a, #b, #c) 21 days after injection. Right: tumor volumes after 21 days (measured as V= (length × width^2)*.5), grouped by CAF strain. Median and SD. CAF1: *shctr* vs *shulk3* n(lesions)= 4 and 6 respectively; CAF3: *shctr* vs *shulk3* n(lesions)= 5 and 4 respectively, unpaired samples, two-tailed equal variance t-test. Scale bar, 5 mm. Matched ear pair comparisons *(shulk3/shctr)* are in Figure S5B. Efficiency of *ulk3* silencing is in Figure S5D.

(B) Left: Immunofluorescence analysis of ear lesions formed by SCC13 cells admixed with CAFs plus/minus *ulk3* silencing with antibodies against p63 or ki67 (green) and pan-keratin (red) for SCC cells identification. Right: quantification of double keratin and p63 or ki67 positive cells for 3 ear pair lesions, using ImageJ and watershed segmentation of digitally acquired images. mean±SEM, n(animals)=3, *p<0.05, two-tailed unpaired t-test. Scale bars, 200μm.

(C) Immunofluorescence analysis of ear lesions in two animals formed by SCC13 cells admixed with *ulk3*-silenced versus control CAF1 with antibodies against endothelial (CD31) and macrophage (CD68) markers, tenascin C (TNC), α-smooth muscle actin (SMA) and periostin (POSTN), with DAPI nuclear staining. The presence of CAFs in the lesions was confirmed with anti vimentin antibodies (VIM). Lower panels: quantification of fluorescence signal for 3 ear pair lesions, using ImageJ software, mean±SEM, n(animals)=3,

Author Manuscript Author Manuscript Author Manuscript Author Manuscript

*<0.05, two-tailed unpaired t-test. Scale bar is 200μM. Highre magnification for TNC and SMA are in Figure S5C.

(D) Summary diagram of the process leading from normal fibroblast to CAF activation, with Ulk3 as critical node as discussed in the text.

See also Figure S5.